

RTDF2009-18016

DETAILED IMPACT ANALYSES FOR DEVELOPMENT OF THE NEXT GENERATION RAIL TANK CAR

Part 1 – Model Development and Assessment of Existing Tank Car Designs

Steven W. Kirkpatrick
Applied Research Associates, Inc.
Mountain View, CA, USA

ABSTRACT

Significant research has been conducted over the past few years to develop improved railroad tank cars that maintain tank integrity for more severe accident conditions than current equipment. The approach taken in performing this research is to define critical collision conditions, evaluate the behavior of current design equipment in these scenarios, and develop alternative strategies for increasing the puncture resistance. The evaluations are being performed with finite element models of the tank cars incorporating a high level of detail. Both laboratory scale and full-scale impact tests were performed to validate the modeling and ultimately compare the effectiveness of current and alternative equipment designs.

This paper describes the development of the detailed finite element model of the tank car and the use of the model for impact and puncture analyses. The validation of the model using the results of the full-scale impact tests is presented. The subsequent application of the model to assess the puncture resistance of existing tank car designs is discussed.

INTRODUCTION

Accident statistics show that the rail industry's safety performance has generally improved over the last few decades. The Federal Railroad Administrations (FRA) Railroad Accident and Incident Reporting System (RAIRS) show that the number of accidents per year with at least one car releasing hazardous materials has decreased significantly over the past 25 years, as shown in Figure 1 [1]. However, a series of three recent accidents or derailments involving the release of hazardous material have focused attention on the structural integrity of railroad tank cars. These events include (1) Minot, ND, on January 18, 2002; (2) Macdona, TX, on June 28, 2004; and (3) Graniteville, SC, on January 6, 2005 [2-4].

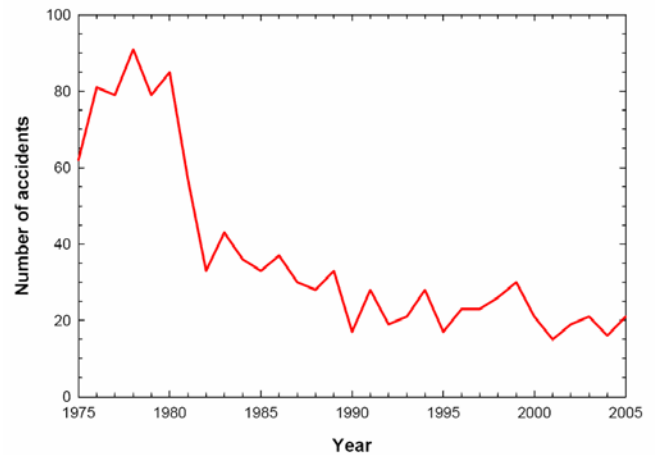
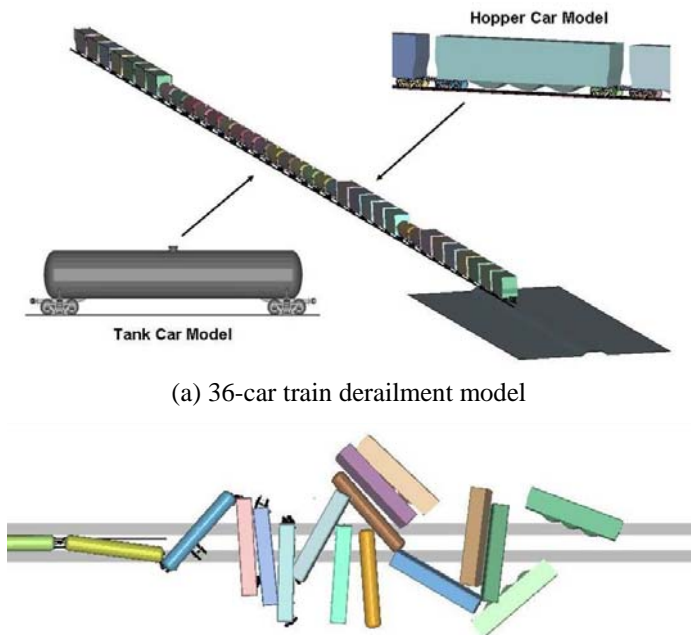


Figure 1. Number of Accidents with at Least One Car Releasing Hazardous Materials [1].

To better define the collision threat, studies have been performed to both evaluate the accident statistics [e.g. 5-7] and analyze the kinematics of freight trains in derailments and collisions [e.g. 8, 9]. Evaluation of the derailments and collisions has shown that these are complex events with a wide range of collisions between the various cars in the train. A 40 mph derailment of a large freight train may involve thirty or more cars and the derailment event would last on the order of a minute before the train comes completely to rest.

An example of a derailment simulation for a 36-car train model is shown in Figure 2. Impacts on tank cars will include both head impacts and side impacts from objects as small as a broken rail to very blunt objects, such as another tank head. Thus, the objective of the tank car development efforts

included increased protection in both head and side impacts for a range of impact conditions.



(a) 36-car train derailment model
 (b) Calculated response 25 seconds after derailment
 Figure 2. Calculated derailment behavior for the 36-car train model [9].

To develop an improved tank car design, the physics of the tank impact response need to be understood. For the purposes of the analyses performed here, the impactor is assumed to be a rigid object. As the impactor strikes the tank, the tank starts to deform. As it deforms, it will develop resisting forces. For a given tank configuration (e.g. tank thickness, internal pressure level) and a given impact condition (e.g. head or side impact, centered or offset impact location) the tank will have a characteristic force-deflection curve, such as that shown in Figure 3. The shape of this force-deflection curve is relatively independent of the size of the impactor. The area under the force-deflection curve is equal to the amount of impact energy that has been dissipated. If the impact speed is sufficiently low, the total energy will be dissipated and the impactor will be safely stopped. If the impact speed is too high, the forces developed will exceed the strength of the tank material and the tank will be punctured. The point at which this failure of the tank is initiated will depend strongly on the size of the impactor.

To absorb additional energy prior to puncture, you can increase the force levels required to deform the tank, increase the displacements that can be experienced prior to puncture initiation, or a combination of both larger forces and larger displacements. The protection strategies are to add external energy absorbing structures and protective layers. These structures may have a larger standoff distance to extend the total displacement and energy dissipation prior tank rupture.

Other protection strategies may be to (1) reinforce the tank system (increasing forces), or (2) blunt the impact loads (increasing the allowable tank displacements prior to rupture).

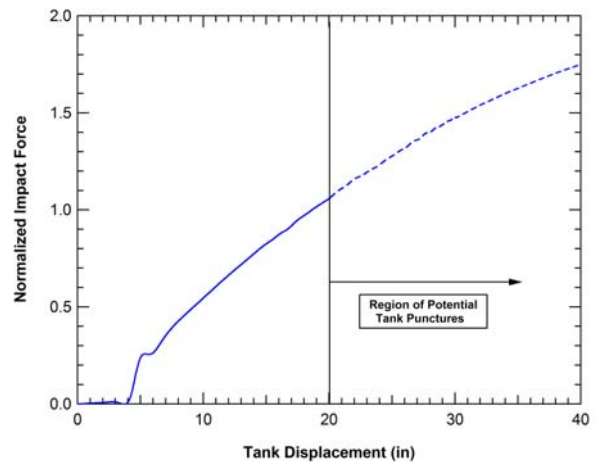


Figure 3. Characteristic force-deflection curve for a tank impact.

A research program was initiated to develop strategies for improving railroad tank cars so they can maintain tank integrity for more severe accident conditions than current equipment. The Next Generation Rail Tank Car (NGRTC) research program was initiated by The Dow Chemical Company (Dow), Union Pacific Railroad, and Union Tank Car Company, working under Memoranda of Cooperation (MOC) with the Federal Railroad Administration, and Transport Canada, and separately with the U.S. Transportation Security Administration.

The NGRTC Project was organized to include a Core Team (consisting of representatives from the signatories to the MOC) and a group of Lead Contractors. The Core Team and Lead Contractors worked together to: 1) evaluate and select candidate materials, components, subsystems and systems with the potential to provide large performance improvements in the safety and security of rail tank cars; 2) select conceptual tank car designs incorporating appropriate materials, components and systems for improved safety and security; and 3) develop and use appropriate models, analytical techniques and testing protocols to demonstrate the efficacy of the tank car concepts. The goal of the NGRTC program was to develop a conceptual tank car that had a five to ten times improvement in the impact energy required to puncture the tank car.

A key effort in this program is the development and application of detailed finite element models of tank cars which can accurately predict the puncture resistance under different impact conditions [10]. These analysis tools were developed and validated for the puncture of the baseline tank cars for both side and head impact conditions. The models were subsequently applied to assess the puncture resistance of various tank car designs.

This paper describes results from the NGRTC project to develop strategies for improving railroad tank cars so they can maintain tank integrity for more severe accident conditions than current equipment. The scope of this effort includes the development of detailed finite element models for tank cars and the use of those models for various impact scenarios to assess puncture energies. A summary of the testing performed under the NGRTC program is also provided in this paper, since it was critical for the development and validation of the puncture modeling capability. The primary emphasis of this paper is on the development and validation of the finite element analyses and the application to current tank car designs. In a companion paper [10], the analysis methods are applied to assess the potential of advanced tank car protection concepts.

BASELINE TANK CAR IMPACT MODEL

The first task in this research was to develop and validate a modeling capability that can be used to analyze the impact response of a tank car. The model developed for the 105J500 chlorine tank car is shown in Figure 4. The model includes all of the primary tank car structures including the jacket and jacket standoffs, commodity tank, manway, bolsters, stub sills, and the addition of the outriggers attached to the draft gear to prevent a post-test rollover of the target tank caused by the rebound off the reaction wall in the impact testing.



Figure 4. Updated model of a 105J500W pressure tank car.

Another feature of the tank impact model was the addition of an explicit model of the lading. The lading model consists of a low strength viscoelastic material that fills the same volume as the slurry lading in the test tank cars. The sloshing of the lading model can be seen in the cutaway view of the predicted impact response shown in Figure 5. This lading modeling approach was established to capture the momentum transfer of the coupled fluid-structure response but minimize effects such as sloshing at the fluid free surface that can cause numerical stability problems.

Full-scale impact tests were performed on tank cars and tank heads [11-13] and the results were used to validate the models. The tests were fully instrumented with accelerometers, string potentiometers, pressure gauges, and strain gauges. These measurements were compared to the model predictions to validate the model. Overall, very good agreement was obtained between the prediction and test for the various measurements made. An example of the agreement is the comparison of the predicted and measured force-deflection curves, shown in Figure 6. This force-deflection curve is an

important characteristic of the tank car for a given impact scenario. The area under the force-deflection curve is the impact energy that is dissipated (the primary measure used to assess the puncture protection levels). The comparison of the force-deflection behaviors shows good agreement between the calculation and the test.

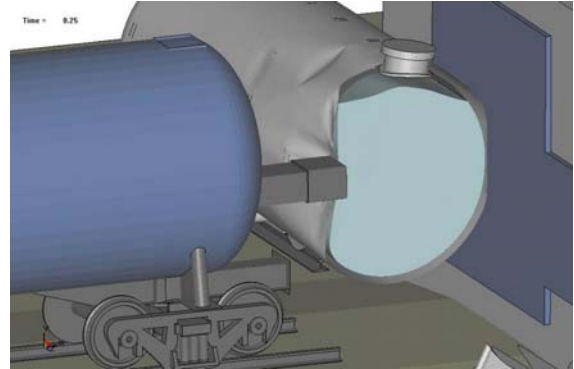


Figure 5. Calculated Test 1 impact response with cutaway showing lading.

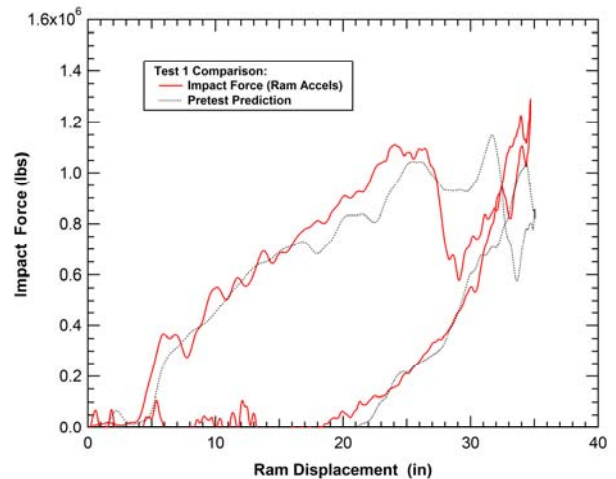


Figure 6. Comparison of the measured and predicted Test 1 force-deflection curves.

MATERIAL DAMAGE AND FAILURE BEHAVIORS

The other necessary component of a predictive tank car puncture modeling capability is a detailed model that can be used to determine the impact damage and failure of the tank and protective system materials. An extensive program of laboratory materials testing was performed to characterize the tank car materials of interest. The tests included various material characterization tests, such as notched tensile tests [14] and combined tension/shear tests [16]. These tests were used to develop the parameters for the material constitutive and failure models. Strain rate effects on the tank car materials were investigated and found to not have a significant effect on the tank puncture behavior. Additional component tests, such as

punch tests and bend tests, were performed to validate the constitutive models.

The material damage and failure model applied is the Bao-Wierzbicki (BW) model [17-19] that defines the material damage development based on the current stress state in the material and the plastic strain increments. This model is an extension of previous ductile damage models [e.g. 20-24] that included the effects of stress state on ductility for primarily tensile stress states. The critical strain function is that proposed in the BW criterion and contains multiple branches depending on the range of stress state, as shown in Figure 7. The critical strain in each branch are governed by the equation

$$\epsilon_c(\sigma_{mean}/\sigma_{eq}) = \begin{cases} \infty & (\sigma_{mean}/\sigma_{eq}) \leq -\frac{1}{3} \\ \frac{A}{1 + 3(\sigma_{mean}/\sigma_{eq})} & -\frac{1}{3} \leq (\sigma_{mean}/\sigma_{eq}) \leq 0 \\ 9(B - A)[(\sigma_{mean}/\sigma_{eq})]^2 + A & 0 \leq (\sigma_{mean}/\sigma_{eq}) \leq \frac{1}{3} \\ \frac{B}{3(\sigma_{mean}/\sigma_{eq})} & \frac{1}{3} \leq (\sigma_{mean}/\sigma_{eq}) \end{cases}$$

where the parameters *A* and *B* can be determined by a series of tests under different stress conditions including notched tensile tests, with specimens of varying notch radii [25], and tensile-shear tests with different ratios of tension to shear stress.

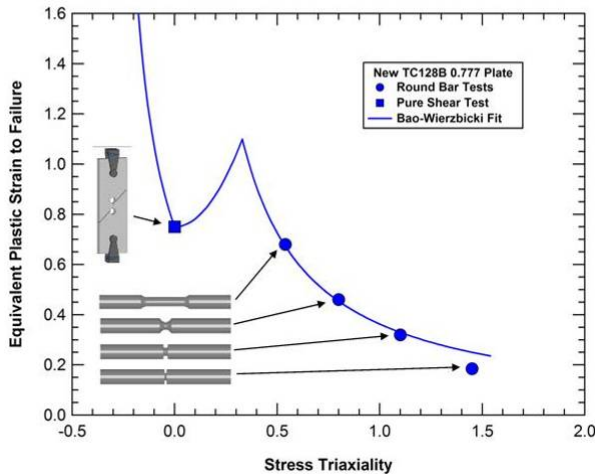


Figure 7. Bao-Wierzbicki failure surface and tests used for model calibration.

Although these material tests were used to develop the constitutive and failure model parameters, the resulting constitutive models were used to simulate the tests. This provides a validation that the material parameters were properly incorporated into the analyses and that the constitutive and failure model is capable of simulating the range of material behaviors under different loading conditions. The first of these material test series was the notched round bar (NRB) tests [14, 26]. The primary material of interest described here is the TC128B tank car steel. A comparison of the calculated and measured stress-strain behavior across the notch for the three

different radii specimens is shown in Figure 8. The comparison shows that the constitutive and damage model were capable of reproducing both the increase in stress level and reduction in ductility that occur as the notch radius is reduced. The BW failure parameters used provide a good correlation to the observed failures of the specimens.

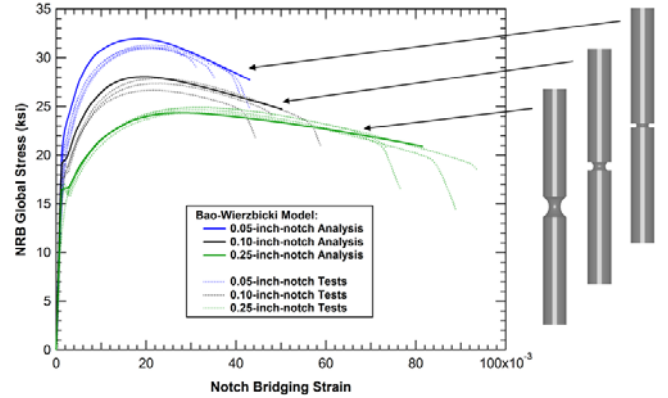


Figure 8. Validation of the notched round bar test behavior for TC128B.

A similar comparison of the calculated and measured load-displacement behaviors for the combined tension/shear tests [16] are shown in Figure 9. The comparison shows again that the constitutive and damage model were capable of reproducing both the decrease in load level and increase in displacement that occur as the orientation was rotated from pure tension to pure shear. The BW failure parameters used provide a good correlation to the observed failures of the specimens.

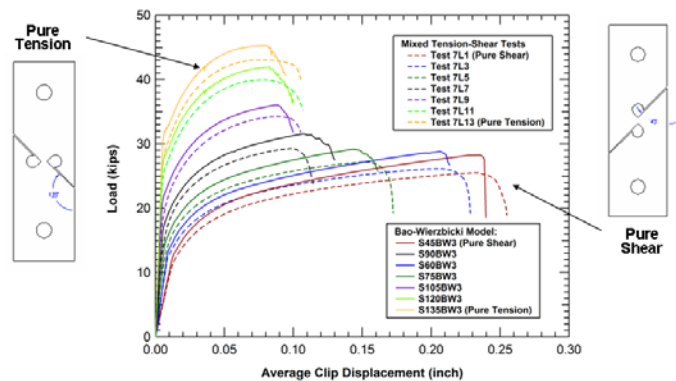


Figure 9. Validation of the combined tensile shear test behavior for TC128B.

For the various steels evaluated in this program, the component punch test was the primary laboratory material test used to validate the constitutive and failure models [27-29]. An example of a model and simulation of a punch test on a 0.488-inch-thick TC128B plate is shown in Figure 10 [28]. The corresponding comparison of measured and calculated punch force-displacement curves for a series of three different tests on the TC128B plate is provided in Figure 11. In addition to the

force-deflection curve, the final profile of the plate specimens after the punch tests were digitized and compared to the analyses. Again, the overall agreement between the testing and analyses was good. This agreement provides a further validation that the BW failure model is appropriate for predicting puncture of the tank cars.

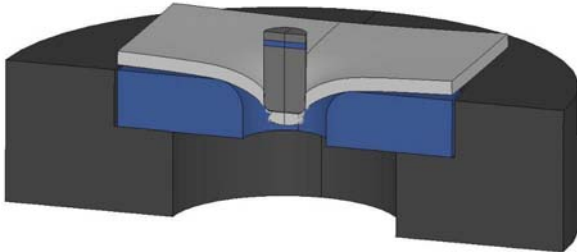


Figure 10. Simulation of the punch test on the thin TC128B plate material.

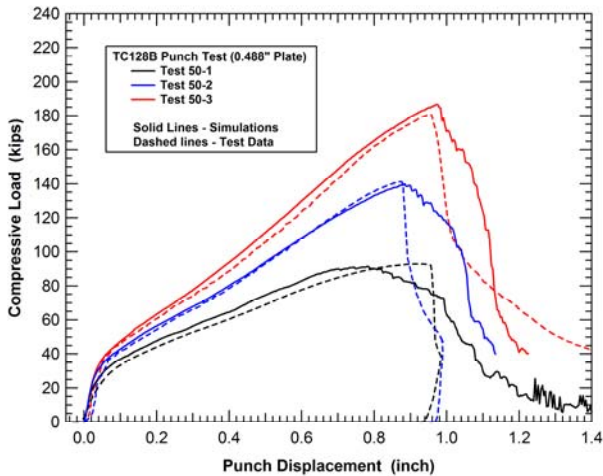


Figure 11. Force-deflection curves for three punch test configurations on TC128B.

TANK CAR PUNCTURE MODELING

The BW failure modeling capability was combined with the tank car model to complete the tank car puncture prediction capability. The approach used was to develop a user-defined constitutive model that was incorporated in the LS-DYNA finite element code [30]. The tank model was also simplified in these puncture analyses to have quarter-symmetry by removing the manway, bolsters and lading. The simulation of the full scale tank car impact test (Test 2 - above the puncture threshold) was performed using the tank puncture model, as shown in Figure 12. The model shown was reflected vertically about the symmetry plane (seen as a line in the figure) for improved visualization of the impact behavior. The impactor in this analysis was a rigid 6x6 inch ram with a 0.50-inch radius around the edges and a total weight of 286,000 lbs. The small rectangular patch of elements under the impactor (already

punctured in Figure 12) is the fracture zone where the BW failure model was applied. The remainder of the tank structure was modeled with 4-node shell elements and a tied shell-to-solid constraint was used at the interface of the two regions.



Figure 12. Simplified tank model analysis with Bao-Wierzbicki failure assessment.

The comparison of the measured and calculated force-deflection behavior for Test 2 with the tank puncture model is provided in Figure 13. The comparison shows overall good agreement between the calculation and test. The peak load at which the tank was punctured was very accurately captured by the model. The measured puncture force was 940,000 lbs and the calculated puncture force was 915,000 lbs. The primary discrepancy of the test and model was a slightly more compliant behavior in the model seen at the large displacements. This difference in compliance could primarily be attributed to the removal of the manway from the tank model in this analysis. As a result of the larger displacements in the analysis, the calculated puncture energy of 1.26 million ft-lbs is higher than the measured puncture energy of 0.87 million ft-lbs.

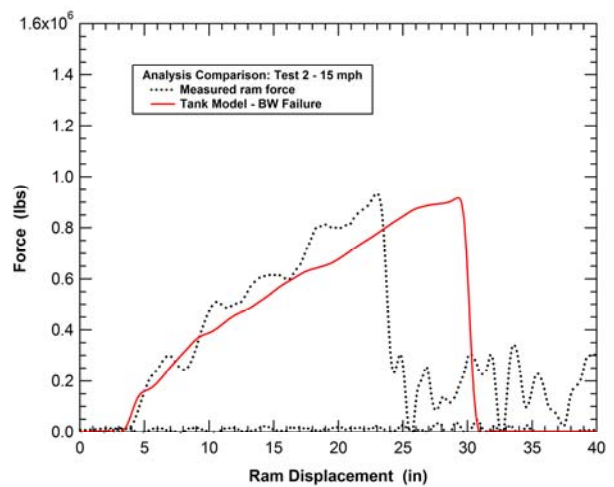


Figure 13. Tank puncture model Test 2 analysis with Bao-Wierzbicki failure assessment.

This combined tank car impact and puncture modeling capability was applied to evaluate a wide range of tank/jacket and head/head shield geometries. The side impact condition was a normal impact centered on the belt line of the tank. The head impact condition was an offset impact point approximately 29 inches vertically downward from the center of the head.

An example head impact and puncture analysis is shown in Figure 14. The head impact analyses included the head, head shield, and a sufficient length of the side shell and jacket to allow for buckling to initiate in the jacket support from the loads transmitted by the head shield, as seen in Figure 14.

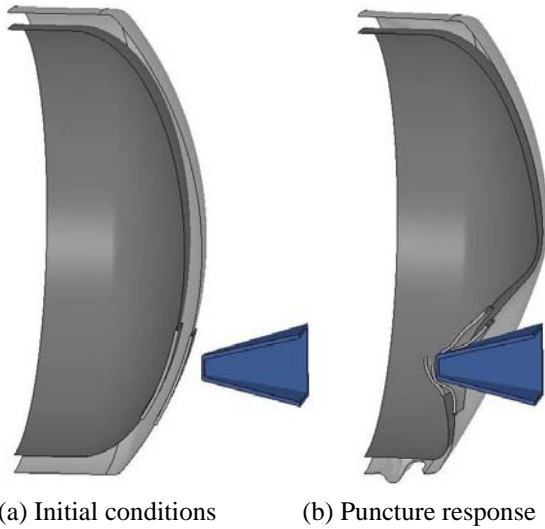


Figure 14. Calculated puncture behavior of a head and head shield.

The calculated puncture force for each of the different head and shell impact analyses are plotted against the combined head and jacket (or head shield) thickness in Figure 15. All of the analyses included in the figure are performed with the 6x6 inch impactor. The figure shows the analyses are mostly consistent with a linear relationship between puncture force and total thickness of the protective layers.

The linear relationship between the puncture force and total tank system thickness provides an indication of the primary failure mechanism initiating the tank puncture. The geometry of the ram impacting and indenting a pressurized tank shell is shown in Figure 16(a). A force balance analysis in the direction of the impact on a patch of tank shell material is shown in Figure 16(b). The forces resisting the impact loads are the pressure on the inside surface of the contact patch and the shear stress around the perimeter of the contact patch. For a 100 psi tank pressure and a 6x6 inch impactor, the pressure load is less than 4 kips on the contact patch. Thus, the average shear stress is approximately equal to the impact force divided by the product of the impactor face perimeter and tank thickness.

The slope of the linear fit in Figure 15 corresponds to an average shear stress in the tank layers around the perimeter of the impactor of 39 ksi. By comparison, the yield and ultimate stress levels of the TC128B in pure shear are 33 ksi and 49 ksi, respectively (approximately 58% of the stress values in pure tension using a Von Mises yield criterion). Thus, the failure mode is primarily exceeding the shear capacity around the perimeter of the impact patch.

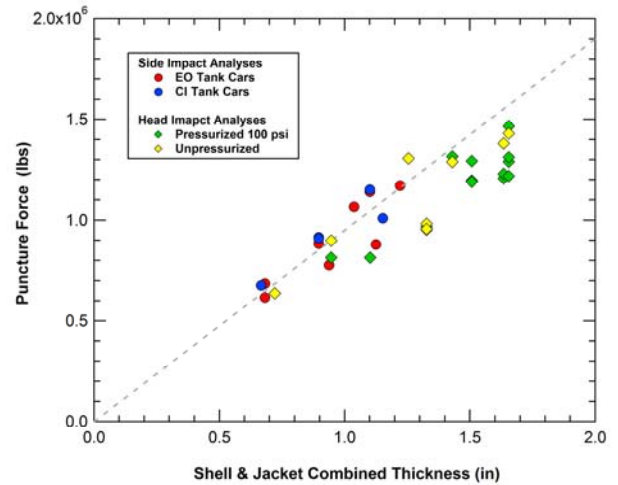
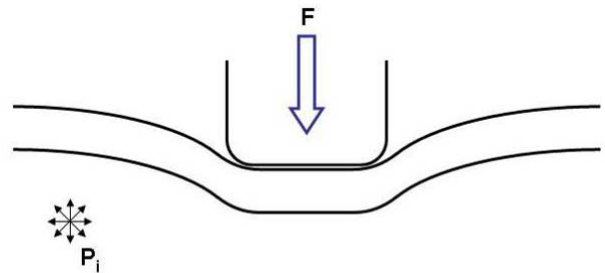
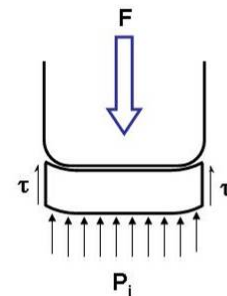


Figure 15. Calculated puncture forces as a function of system thickness.



(a) Geometry of the tank indentation



(b) Free body diagram for the tank contact patch

Figure 16. Loading and failure mechanism for the tank impact and puncture.

The calculated puncture forces for pressurized heads and the thicker head systems tended to fall slightly below the linear fit in Figure 15. The proposed mechanism for these lower forces is that, for the stiffer head systems, the offset impact creates a larger stress concentration along the upper edge of the impactor face and the failure initiates at that location at a lower total force. The more compliant head systems allow for a larger dent to form and the impactor develops a more uniform stress distribution in the impact patch around the ram face perimeter.

The calculated puncture energies for all of the side and head impact analyses are plotted against the combined thickness of the system in Figure 17 (6x6 inch impactor only). When comparing all of the puncture energies the data falls into four separate groups that are distinguished by the impact type (side or head) and the tank pressure. Again, the comparison indicates that the total thickness is the relative parameter that determines puncture energy for a given impact condition and pressure level, indicating that a retrofit design with an increased jacket thickness should provide equivalent protection to a thicker commodity tank systems with equivalent combined shell and jacket thicknesses.

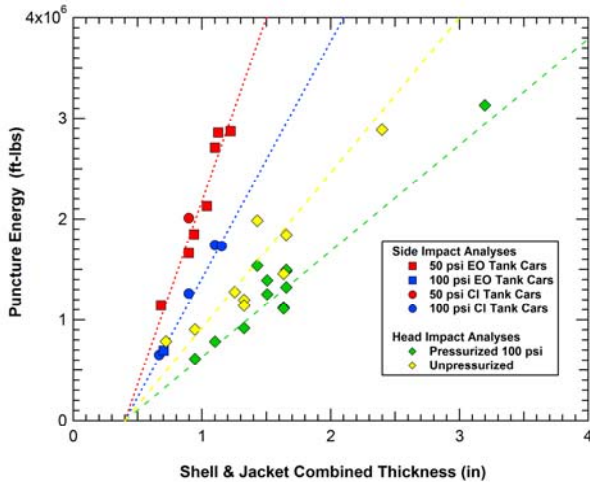


Figure 17. Calculated puncture energies as a function of system thickness.

The above correlation of the system thickness and puncture energy can be converted to assess system requirements for a given impact scenario. The relationship between the impact speed and impact energy for the 295,000 lb ram car is provided in Figure 18. This impact energy is proportional to the mass of the object so a 286,000 ram car would have energies that are three percent lower than those in Figure 18. This relationship between speed and impact energy can be combined with the linear fits between system thickness and puncture energy (shown in Figure 17) to determine the required system thickness to resist puncture for a specified impact speed.

Examples of the pressurized (100 psi) CI tank car thickness requirements to resist a puncture of the 6x6 inch impactor at various impact speeds is shown in Figure 19 for both side and

head impacts. The figure shows that as the impact speed increases, the system thickness required begins to increase rapidly. A 25 mph side impact would require approximately three inches of steel to prevent puncture and a 30 mph head impact would require more than six inches of steel. Obviously, these protection levels are not achievable with a traditional tank car design approach while maintaining a tank car that is economically viable as a result of both the initial tank car cost and the drastically reduced lading capacity.

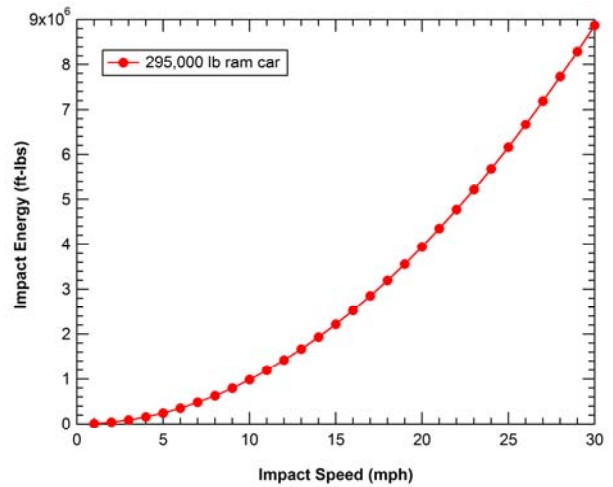


Figure 18. Relationship between impact speed and kinetic energy for the ram car.

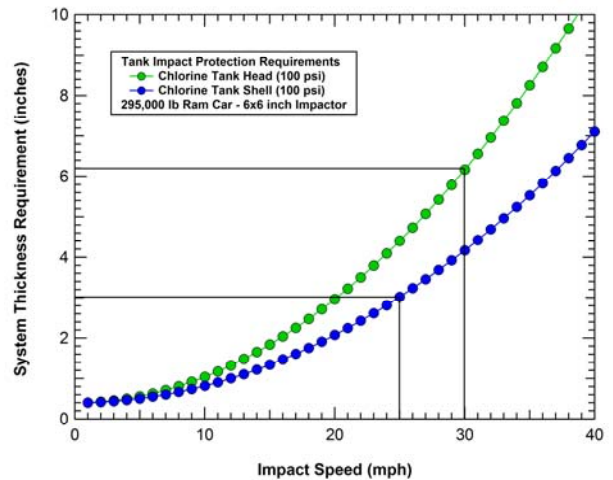


Figure 19. Puncture prevention thickness requirements for various impact speeds.

The analyses demonstrate that the 25 and 30 mph impact protection levels are not feasible for the 6x6 inch impactor. However, the additional analyses demonstrate that they would be achievable with a larger ram size. The puncture energies from analyses of side impacts on 500 lb and 600 lb tanks using 6-inch, 9-inch, and 12-inch square impactors are shown in Figure 20. The figure shows that the 25 mph ram car impact (6

million ft-lb impact energy from Figure 18) is approximately equivalent to the puncture energy of the 600 lb tank car impacted by the 12x12 inch ram.

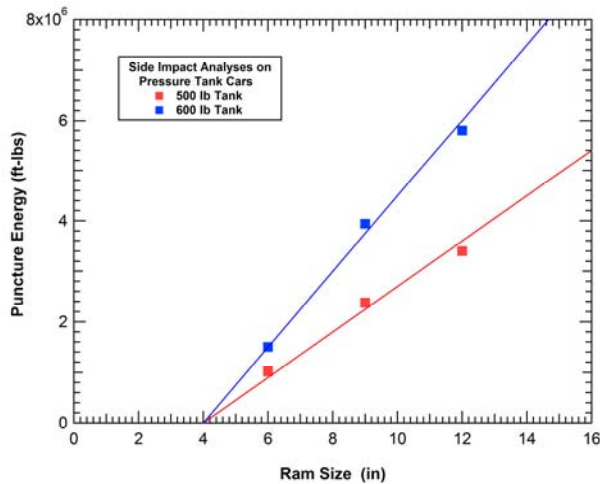


Figure 20. Summary of puncture energies for chlorine tank cars for various impactor sizes.

SUMMARY AND CONCLUSIONS

This paper describes the development and validation of detailed analysis methodologies for predicting the impact response and puncture potential of railroad tank cars. The primary impact threat considered was a 6x6 inch impactor. For the systems analyzed here, this impactor acts like a relatively small punch and the primary failure mode is a punch shear failure around the perimeter of the impactor face.

Analyses of traditional tank car designs show that the puncture force for the 6x6 inch impactor is roughly proportional to the combined thickness of the tank and jacket (or head and head shield). Thus, a reasonable amount of additional puncture protection can be achieved by increasing the thickness of the tank or increasing the thickness of the jacket and head shield.

The impact energy dissipated prior to puncture depends on the compliance of the tank under the specific impact conditions. A more compliant tank or impact orientation allows for a larger indentation length before the tank exceeds the puncture force threshold and, as a result, dissipates a larger amount of impact energy. The side impact orientation was more compliant than head impacts and increasing the pressure in the tank reduces the compliance of the system.

ACKNOWLEDGMENTS

The contents of this paper are based primarily on work funded by The Dow Chemical Company, on behalf of the Next Generation Rail Tank Car (NGRTC) Project. The development of the puncture modeling methodologies and the testing used to validate the models and develop the constitutive and failure models were all performed under the NGRTC project. The

analyses of the Ethylene Oxide (EO) tank cars were funded by the American Chemistry Council, Inc., on behalf of its Ethylene Oxide Panel.

REFERENCES

1. Tyrell, D.C., Jeong, D.Y., Jacobsen, K., Martinez, E., "Improved Tank Car Safety Research," Proceedings of the 2007 ASME Rail Transportation Division Fall Technical Conference, RTDF2007-46013, September 2007.
2. National Transportation Safety Board, 2004: "Derailment of Canadian Pacific Railway Freight Train 292-16 and Subsequent Release of Anhydrous Ammonia Near Minot, North Dakota; January 18, 2002," Railroad Accident Report NTSB/RAR-04/01.
3. National Transportation Safety Board, 2006: "Collision of Union Pacific Railroad Train MHOTU-23 with BNSF Railway Company Train MEAP-TUL-126-D with Subsequent Derailment and Hazardous Materials Release, Macdona, Texas, June 28, 2004," Railroad Accident Report NTSB/RAR-06/03.
4. National Transportation Safety Board, 2005: "Collision of Norfolk Southern Freight Train 192 with Standing Norfolk Southern Local Train P22 with Subsequent Hazardous Materials Release at Graniteville, South Carolina, January 6, 2005," Railroad Accident Report NTSB/RAR-05/04.
5. Barkan, Christopher P.L., Satis V. Ukkusuri, S. Travis Waller, "Optimizing the design of railway tank cars to minimize accident-caused releases", Computers & Operations Research, (2005 Elsevier Ltd).
6. Saat, Mohd Rapik, Christopher P.L. Barkan, "Release Risk and Optimization of Railroad Tank Car Safety Design", Transportation Research Record: Journal of the Transportation Research Board (2005).
7. Saat, Mohd Rapik, Christopher P.L. Barkan, "Release Risk as Metric for Evaluating Tank Car Safety Performance", Saat & Barkan 05-1826.
8. Jeong, D.Y., Lyons, M.L., Orringer, O., Perlman, A.B., 2007: "Equations of Motion for Train Derailment Dynamics," Proceedings of 2007 ASME Rail Transportation Division Fall Technical Conference, Paper No. RTDF2007-46009.
9. S.W. Kirkpatrick, B.D. Peterson, and R.A. MacNeill, "Finite Element Analysis of Train Derailments," ICrash2006. Proceedings of the International Crashworthiness Conference, July 4-7, 2006, Athens, Greece.
10. S.W. Kirkpatrick, "Detailed Impact Analyses for Development of the Next Generation Rail Tank Car - Part 2 –Development of Advanced Tank Car Protection Concepts," Proceedings of the ASME 2009 Rail Transportation Division Fall Conference, Paper No. RTDF2009-18017, October 20-21, 2009, Ft. Worth, Texas, USA.
11. Matthew Witte and Satima Anankitpaiboon, "Fully Instrumented Side Impact Test of Tank Car 3069," Transportation Technology Center, Inc. Report No. P-07-033, October 8, 2007.
12. Matthew Witte and Satima Anankitpaiboon, "Second Fully Instrumented Tank Car Baseline Side Impact Test of Tank Car

- 3074," Transportation Technology Center, Inc. Report No. P-07-034, October 8, 2007.
13. Russell Walker, Greg Garcia, Satima Anankitpaiboon, and Kari Gonzales, "Tank Car Head Baseline Component Test," Transportation Technology Center, Inc. Report No. P-08-009, April 2008.
 14. Pete McKeighan, "Notched Tensile Properties of Tank Car Material from Full Scale Test No. 1 (Car No. 3069) and Test No. 2 (3074) Oriented in the Transverse Direction," NGRTC Project Memorandum, Southwest Research Institute, 20 November 2007.
 15. Pete McKeighan, "Notched Tensile Properties of Thickest TC128B Tank Car Material from Material Inventory for Fabricating Test Specimens," NGRTC Project Memorandum, Southwest Research Institute, 6 December 2007.
 16. Pete McKeighan, "Shear Tests on TC128B Normalized Material of Two Different Thicknesses," NGRTC Project Memorandum, Southwest Research Institute, December 2007.
 17. Bao, Y., and Wierzbicki, T., "On Fracture Locus in the Equivalent Strain and Stress Triaxiality Space," *International Journal of Mechanical Sciences* 46, 81-98.
 18. Bao, Y., and Wierzbicki, T., "A Comparative Study on Various Ductile Crack Formation Criteria," *Journal of Engineering Materials and Technology* 126, 314-324.
 19. Young-Woong Lee and Tomasz Wierzbicki, "Quick Fracture Calibration for Industrial Use," Massachusetts Institute of Technology Impact & Crashworthiness Laboratory, Report No: 115, August 2004.
 20. Beremin, F. M., 1981, "Study of Fracture Criteria for Ductile Rupture of A508 Steel," in *Advances in Fracture Research (ICF5)*, D. François, Ed., Pergamon Press, pp. 809-816.
 21. Lemaitre, J., 1986, "Local Approach of Fracture," *Engineering Fracture Mechanics*, Vol. 25, pp. 523-537.
 22. Mudry, F., 1985, "Methodology and Applications of Local Criteria for Prediction of Ductile Tearing," *Elastic-Plastic Fracture Mechanics*, L. H. Larson, ed., ECSC, EEC, EAEC, Brussels and Luxembourg, Belgium, pp. 263-283.
 23. Hancock, J. W. and Mackenzie, A. C., 1976, "On the Mechanisms of Ductile Failure in High-Strength Steels Subjected to Multiaxial Stress States," *Journal of the Mechanics and Physics of Solids*, 24, pp. 147-169.
 24. Rice, J. R., and Tracey, D. M., 1969, "On the Ductile Enlargement of Voids in Triaxial Stress Fields," *J. Mech. Phys. Solids*, 17, 201-217.
 25. Mackenzie, A. C., Hancock, J. W., and Brown, D. K., 1977, "On the Influence of State of Stress on Ductile Failure Initiation in High-Strength Steels," *Eng. Fracture Mechanics*, 9, 167-188.
 26. Pete McKeighan, "Tensile Properties and Stress-Strain Behavior of Various Steel Products Used in Fabricating Test Specimen for the NGRTC Program," NGRTC Project Memorandum, Southwest
 27. Pete McKeighan, "Puncture Tests on Jacket Material (A1011, 90X) and Normalized TC128B Shell Material (two thicknesses)- Revised," NGRTC Project Memorandum, Southwest Research Institute, 17 December 2007.
 28. Pete McKeighan, "Puncture Behavior of 0.48-inch Thick A516 Material," NGRTC Project Memorandum, Southwest Research Institute, 12 April 2008.
 29. Pete McKeighan, "Puncture Properties of Different 90x Stacked Layers and a Composite Structure," NGRTC Project Memorandum, Southwest Research Institute, 23 March 2008.
 30. "LS-DYNA Keyword User's Manual," Livermore Software Technology Corporation, Version 970, April 2003.